Measurement of J/ψ decays into $\Lambda\bar{\Lambda}$ $\pi^+\pi^-$*

M. Ablikim(阿布里克木·麦迪娜)[1] J. Z. Bai(白景芝)[1] Y. Bai(白羽)[1] Y. Ban(班勇)[11] X. Cai(蔡啸)[1]
H. F. Chen(陈宏芳)[17] H. S. Chen(陈和生)[1] J. C. Chen(陈江川)[1] J. Chen(陈进)[1]
Y. B. Chen(陈元柏)[1] Y. P. Chu(初元萍)[1] Y. S. Dai(戴又善)[19] Z. Y. Deng(邓子艳)[1]
S. X. Du(杜书先)[1a] J. Fang(方建)[1] C. D. Fu(傅成栋)[1] Y. Gao(高原宁)[15] Y. T. Gu(顾运厅)[4]
Z. J. Guo(郭子敬)[16b] F. A. Harris[16] K. L. He(何康林)[1] M. He(何瑁)[13] Y. K. Heng(衡月昆)[1]
H. M. Hu(胡海明)[1] T. Hussain[1c] T. Hu(胡涛)[1] G. S. Huang(黄光顺)[17] X. T. Huang(黄性涛)[13]
Y. P. Huang(黄燕萍)[1] T. Hussain[1c] X. B. Ji(季晓斌)[1] X. S. Jiang(江晓山)[1] J. B. Jiao(焦健斌)[13]
D. P. Jin(金大鹏)[1] S. Jin(金山)[1] G. Li(李刚)[1] H. B. Li(李海波)[1] J. Li(李金)[1] L. Li(李蕾)[1]
R. Y. Li(李仁英)[1] W. D. Li(李卫东)[1] W. G. Li(李卫国)[1] X. L. Li(李晓玲)[13] X. N. Li(李小男)[1]
X. Q. Li(李学潜)[10] Y. F. Liang(梁勇飞)[14] B. J. Liu(刘北江)[1] C. X. Liu(刘春秀)[1] Fang Liu(刘芳)[1]
Feng Liu(刘峰)[6] H. B. Liu(刘宏邦)[4] H. M. Liu(刘怀民)[1] J. P. Liu(刘觉平)[18] Q. Liu(刘倩)[16d]
R. G. Liu(刘荣光)[1] Z. A. Liu(刘振安)[1] F. Lu(吕峰)[1] G. R. Lu(鲁公儒)[5] J. G. Lu(吕军光)[1]
X. L. Luo(罗成林)[9] F. C. Ma(马凤才)[8] H. L. Ma(马海龙)[1] Q. M. Ma(马秋梅)[1] M. Q. A. Malik[1c]
Z. P. Mao(毛泽普)[1] X. H. Mo(莫晓虎)[1] J. Nie(聂晶)[1] S. L. Olsen[12] R. G. Ping(平荣刚)[1]
J. F. Qiu(邱进发)[1] G. Rong(荣刚)[1] X. D. Ruan(阮向东)[4] L. Y. Shan(单连友)[1] L. Shang(尚雷)[1]
C. P. Shen(沈成平)[16e] X. Y. Shen(沈肖雁)[1] H. Y. Sheng(盛华义)[1] S. S. Sun(孙海生)[1]
S. S. Sun(孙胜森)[1] Y. Z. Sun(孙永昭)[1] Z. J. Sun(孙志嘉)[1] X. Tang(唐晓)[1] J. P. Tian(田俊平)[15]
G. S. Varner[16] X. Wan(万霞)[1] L. Wang(王岚)[1] L. L. Wang(王亮亮)[1] L. S. Wang(王灵淑)[1]
P. Wang(王平)[1] P. L. Wang(王佩良)[1] Y. F. Wang(王贻芳)[1] Z. Wang(王铮)[1] Z. Y. Wang(王至勇)[1]
C. L. Wei(魏诚林)[1] D. H. Wei(魏代会)[3] N. Wu(吴宁)[1] G. F. Xu(许国发)[1] X. P. Xu(徐新平)[6f]
Y. Xu(徐晔)[10] M. L. Yan(阎沐霖)[17] H. X. Yang(杨洪勋)[1] M. Yang(杨明)[1] Y. X. Yang(杨永栩)[3]
M. H. Ye(叶铭汉)[2] Y. X. Ye(叶云秀)[17] C. X. Yu(喻纯旭)[10] C. Z. Yuan(苑长征)[1] Y. Yuan(袁野)[1]
Y. Zeng(曾云)[7] B. X. Zhang(张丙新)[1] B. Y. Zhang(张炳云)[1] C. C. Zhang(张长春)[1]
D. H. Zhang(张达华)[1] H. Q. Zhang(张华桥)[1] H. Y. Zhang(章红宇)[1] J. W. Zhang(张家文)[1]
J. Y. Zhang(张建勇)[1] X. Y. Zhang(张学尧)[13] Y. Y.Zhang(张一云)[14] Z. P. Zhang(张子平)[17]
J. W. Zhao(赵京伟)[1] M. G. Zhao(赵明刚)[10] P. P. Zhao(赵平平)[1] Z. G. Zhao(赵政国)[17]
B. Zheng(郑波)[1] H. Q. Zheng(郑海青)[11] J. P. Zheng(郑建平)[1] Z. P. Zheng(郑志鹏)[1]
B. Zhong(钟彬)[1] L. Zhou(周莉)[1] K. J. Zhu(朱科军)[1] Q. M. Zhu(朱启明)[1]
X. W. Zhu(朱兴旺)[1] Y. S. Zhu(朱永生)[1] Z. A. Zhu(朱自安)[1] B. S. Zou(邹冰松)[1]
(BESⅡ collaboration)

[1] Institute of High Energy Physics, Beijing 100049, China
[2] China Center of Advanced Science and Technology, Beijing 100190, China
[3] Guangxi Normal University, Guilin 541004, China
[4] Guangxi University, Nanning 530004, China
[5] Henan Normal University, Xinxiang 453007, China

Received 16 July 2012, Revised 16 August 2012

*Supported by National Natural Science Foundation of China (10491300, 10225524, 10225525, 10425523, 10625524, 10521003, 10821063, 10825524), Chinese Academy of Sciences (KJ 95T-03), 100 Talents Program of CAS (U-11, U-24, U-25), Knowledge Innovation Project of CAS (U-602, U-34) (IHEP), National Natural Science Foundation of China (10775077, 10225522) (Tsinghua University), and Department of Energy (DE-FG02-04ER41291) (U. Hawaii)

[6] Huazhong Normal University, Wuhan 430079, China
[7] Hunan University, Changsha 410082, China
[8] Liaoning University, Shenyang 110036, China
[9] Nanjing Normal University, Nanjing 210046, China
[10] Nankai University, Tianjin 300071, China
[11] Peking University, Beijing 100871, China
[12] Seoul National University, Seoul, 151-747 Korea
[13] Shandong University, Jinan 250100, China
[14] Sichuan University, Chengdu 610064, China
[15] Tsinghua University, Beijing 100084, China
[16] University of Hawaii, Honolulu, Hawaii 96822, USA
[17] University of Science and Technology of China, Hefei 230026, China
[18] Wuhan University, Wuhan 430072, China
[19] Zhejiang University, Hangzhou 310027, China
[a] now at Zhengzhou University, Zhengzhou 450001, China
[b] now at Johns Hopkins University, Baltimore, MD 21218, USA
[c] now at Centre for High Energy Physics, University of the Punjab, Lahore-54590, Pakistan
[d] now at Graduate University of Chinese Academy of Sciences, Beijing 100049, China
[e] now at Nagoya University, Nagoya, Japan
[f] now at Soochow University, Suzhou 215006, China

Abstract: Based on 58 million J/ψ events collected by the BES II detector at the BEPC, $J/\psi \to \Lambda\bar{\Lambda}\pi^+\pi^-$ is observed for the first time. The branching fraction is measured to be $Br(J/\psi \to \Lambda\bar{\Lambda}\pi^+\pi^-) = (4.30 \pm 0.13 \pm 0.99) \times 10^{-3}$, excluding the decays to intermediate states, namely $J/\psi \to \Xi^-\bar{\Xi}^+$, $J/\psi \to \Sigma(1385)^-\bar{\Sigma}(1385)^+$, and $J/\psi \to \Sigma(1385)^+\bar{\Sigma}(1385)^-$. The branching fractions for these intermediate resonance channels are measured to be: $Br(J/\psi \to \Xi^-\bar{\Xi}^+) = (0.90 \pm 0.03 \pm 0.18) \times 10^{-3}$, $Br(J/\psi \to \Sigma(1385)^-\bar{\Sigma}(1385)^+) = (1.23 \pm 0.07 \pm 0.30) \times 10^{-3}$, and $Br(J/\psi \to \Sigma(1385)^+\bar{\Sigma}(1385)^-) = (1.50 \pm 0.08 \pm 0.38) \times 10^{-3}$, respectively. The angular distribution is of the form $\frac{dN}{d(\cos\theta)} \propto (1 + \alpha\cos^2\theta)$ with $\alpha = (0.35 \pm 0.29 \pm 0.06)$ for $J/\psi \to \Xi^-\bar{\Xi}^+$, $\alpha = (-0.54 \pm 0.22 \pm 0.10)$ for $J/\psi \to \Sigma(1385)^-\bar{\Sigma}(1385)^+$, and $\alpha = (-0.35 \pm 0.25 \pm 0.06)$ for $J/\psi \to \Sigma(1385)^+\bar{\Sigma}(1385)^-$.

Key words: baryonic decays, branching fraction, alpha distribution

PACS: 25.40.Cm, 28.75.Gz, 21.60.-n **DOI:** 10.1088/1674-1137/36/11/001

1 Introduction

The decays of J/ψ into baryon pairs ($B\bar{B}$), which are predicted to proceed via the annihilation of the constituent $c\bar{c}$ into three gluons, have been studied in Refs. [1, 2].

In this paper, we report a measurement of the branching fraction of $J/\psi \to \Lambda\bar{\Lambda}\pi^+\pi^-$, which has not been previously measured. Also, we find three intermediate resonances $J/\psi \to \Xi^-\bar{\Xi}^+$, $J/\psi \to \Sigma(1385)^-\bar{\Sigma}(1385)^+$, and $J/\psi \to \Sigma(1385)^+\bar{\Sigma}(1385)^-$, and their branching fractions are measured. By using hadron helicity conservation, the angular distribution of $e^+e^- \to J/\psi \to B\bar{B}$ can be expressed as:

$$\frac{dN}{d\cos\theta} \propto (1 + \alpha\cos^2\theta),$$

where θ is the angle between the baryon and the beam direction of the positron in the center-of-mass system. We have measured the angular parameter, α, for these $B\bar{B}$ decays. Decay rates of $J/\psi \to B_8\bar{B}_8$ (B_8 : octet baryon) and $J/\psi \to B_{10}\bar{B}_{10}$ (B_{10} : decouplet baryon) have been discussed, and α values have also been measured in different experiments [1–6]. In addition, theoretical values of α have also been calculated [7, 8]. It is important to note that for J/ψ decays into baryon and anti-baryon pairs, the velocity of the baryon is non-relativistic, so α can take any value between -1 and 1.

2 The BES II detector

BES was a conventional solenoidal magnetic detector that is described in detail in Ref. [9]. BES II is the upgraded version of the BES detector [10]. A 12-layer vertex chamber (VC) surrounding the beryllium beam pipe provids track and trigger information. A forty-layer main drift chamber (MDC) located just outside the VC provides measurements of charged particle trajectories covering 85% of 4π; it also provides ionization energy loss (dE/dx) measurements which are used for particle identification (PID). A momentum resolution of $0.0178\sqrt{1+p^2}$ (p in GeV/c) and a dE/dx resolution for hadronic tracks of $\sim 8\%$ are obtained. The time of flight (TOF)

of charged particles is measured with an array of 48 scintillation counters surrounding the MDC. The time resolution is about 200 ps for hadrons. Outside the TOF counters, a 12 radiation long, lead-gas barrel shower counter (BSC), measures the energies and positions of electrons and photons. The solid angle covered is over 80%, and the energy resolutions of $\sigma_E/E = 0.22/\sqrt{E}$ (E in GeV) and the position resolutions, $\sigma_\phi = 7.9$ mrad, and $\sigma_z = 2.3$ cm are obtained. Outside the solenoidal coil, which provides a 0.4 T magnetic field over the tracking volume, three double-layer muon counters instrumented in the flux return identified muons with momenta greater than 500 MeV/c. The BESII detector was de-commissioned in 2004.

3 The Monte Carlo simulation and selection criteria

The Monte Carlo (MC) simulations are performed using a GEANT3 based program (SIMBES) with detailed consideration of the detector geometry and response. The consistency between data and MC simulations has been checked in many J/ψ and ψ(2S) decays with reasonable agreement. Details are described in Ref. [11].

The exclusive MC sample of $J/\psi \to \Lambda\bar{\Lambda}\pi^+\pi^- \to p\bar{p}\pi^+\pi^-\pi^+\pi^-$ is generated with a pure phase space model. The decays of $J/\psi \to \Xi^-\bar{\Xi}^+$, $J/\psi \to \Sigma(1385)^-\bar{\Sigma}(1385)^+$ and $J/\psi \to \Sigma(1385)^+\bar{\Sigma}(1385)^-$ are generated with the angular distribution parameter α consistent with the measured values.

The reconstructed $J/\psi \to \Lambda\bar{\Lambda}\pi^+\pi^-$ candidate events are required to have six charged tracks, and the total charge must be equal to zero. In order to ensure well-measured momenta and reliable particle identification, all the tracks are required to be reconstructed in the main drift chamber with a good helix fit. Each track is required to satisfy $|\cos\theta| < 0.8$, where θ is the polar angle, and originate from the beam interaction region, which is defined by $R_{xy} < 0.15$ m and $|z| < 0.45$ m, where R_{xy} and z are respectively the distances in the xy plane of the point of closest approach of the charged track to the beamline and the z offset from the interaction point. Particle identification for the proton and antiproton is performed using $\mathrm{d}E/\mathrm{d}x$ and TOF information. We select the Λ and $\bar{\Lambda}$ at the same time from all possible pπ combinations. If there is more than one combination, the combination with the minimum $|M_{p\pi^-} - M_\Lambda| + |M_{\bar{p}\pi^+} - M_{\bar{\Lambda}}|$ is chosen, where M_Λ is the nominal mass of Λ. The Λ and $\bar{\Lambda}$ candidates are selected by requiring $|M_{p\pi^-} - M_\Lambda| < 0.008$ GeV/c^2 and $|M_{\bar{p}\pi^+} - M_{\bar{\Lambda}}| < 0.008$ GeV/c^2, respectively.

Imposing energy-momentum conservation, a four constraint (4-C) kinematic fit is made under the hypothesis of $J/\psi \to p\bar{p}\pi^+\pi^-\pi^+\pi^-$. The χ^2 distributions of data and MC are consistent with each other so a loose requirement $\chi^2 < 50$ is used. Possible background channels are $J/\psi \to \Xi(1530)^-\bar{\Xi}^+$, $J/\psi \to 3(\pi^+\pi^-)\pi^0$, $J/\psi \to 2(\pi^+\pi^-)K^+K^-$, $J/\psi \to 3(\pi^+\pi^-)$, $J/\psi \to 3(\pi^+\pi^-)\eta$, $J/\psi \to \Delta(1232)^{++}\Delta(1232)^{--}$, $J/\psi \to \Delta(1232)^{++}\bar{p}\pi^-$, and $J/\psi \to \Sigma(1385)^-\bar{\Sigma}^+$, but no major backgrounds for the $J/\psi \to \Lambda\bar{\Lambda}\pi^+\pi^-$ are found.

4 The study of intermediate resonances

There are three intermediate resonances clearly seen in the selected $\Lambda\bar{\Lambda}\pi^-\pi^+$ events. As shown in the scatter plot of $\Lambda\pi^-$ versus $\bar{\Lambda}\pi^+$ mass in Fig. 1, there are two accumulations of events. The accumulation of events near 1.321 GeV/c^2 corresponds to $\Xi(1321)^-$ ($\bar{\Xi}(1321)^+$), and the accumulation near 1.385 GeV/c^2 is $\Sigma(1385)^-$ ($\bar{\Sigma}(1385)^+$). From this plot, two modes with intermediate resonances are very clearly seen; $J/\psi \to \Xi^-\bar{\Xi}^+$ and $J/\psi \to \Sigma(1385)^-\bar{\Sigma}(1385)^+$.

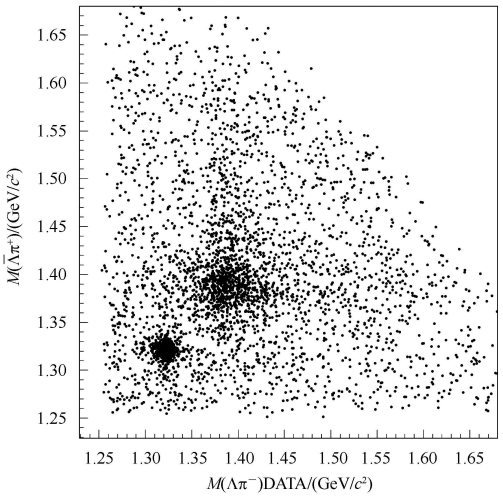

Fig. 1. The scatter plot of $M(\Lambda\pi^-)$ versus $M(\bar{\Lambda}\pi^+)$ mass for data. There are accumulations of events for $\Xi^-\bar{\Xi}^+$ and $\Sigma(1385)^-\bar{\Sigma}(1385)^+$ near the masses of 1.321 GeV/c^2 and 1.385 GeV/c^2, respectively.

The other intermediate resonance may be seen in the scatter plot of the $\Lambda\pi^+$ versus the $\bar{\Lambda}\pi^-$ mass, shown in Fig. 2. The accumulation of events near 1.385 GeV/c^2 is $\Sigma(1385)^+$ ($\bar{\Sigma}(1385)^-$). From this plot, it is clear that there is another intermediate resonance, $J/\psi \to \Sigma(1385)^+\bar{\Sigma}(1385)^-$.

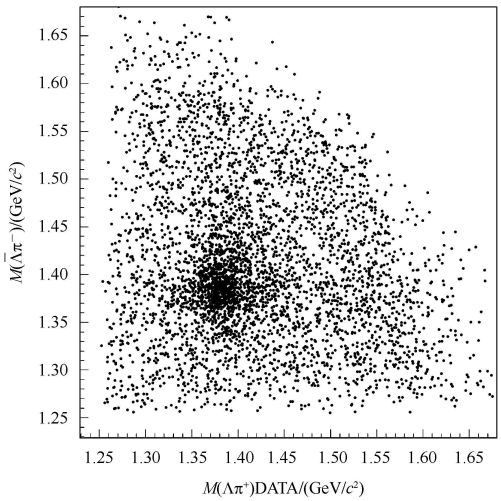

Fig. 2. The scatter plot of $M(\Lambda\pi^+)$ versus $M(\bar{\Lambda}\pi^-)$ for data. The accumulation of events near 1.385 GeV/$c^2$is $\Sigma(1385)^+\bar{\Sigma}(1385)^-$. From this plot, it is clear that there is another intermediate resonance $\mathrm{J/\psi}\to\Sigma(1385)^+\bar{\Sigma}(1385)^-$.

4.1 The observation of $\bar{\Xi}(1321)^+$ and $\bar{\Sigma}(1385)^+$

For $\mathrm{J/\psi}\to\Xi^-\bar{\Xi}^+\to(\Lambda\pi^-)(\bar{\Lambda}\pi^+)\to(\mathrm{p}\pi^-\pi^-)(\bar{\mathrm{p}}\pi^+\pi^+)$, the $\Xi^-(\bar{\Xi}^+)$ is reconstructed with $\Lambda\pi^-(\bar{\Lambda}\pi^+)$, and the $\Lambda(\bar{\Lambda})$ selection criteria are the same as above.

The invariant mass of $\Lambda\pi^-$ is plotted in Fig. 3 requiring $|M(\bar{\Lambda}\pi^+)-1.321|<0.012$ GeV/c^2 to select the signal and $|M(\bar{\Lambda}\pi^-)-1.383|>0.054$ GeV/c^2 and $|M(\Lambda\pi^+)-1.383|>0.054$ GeV/c^2 to veto $\mathrm{J/\psi}\to\Sigma(1385)^+\bar{\Sigma}(1385)^-$. The distribution is fitted with a histogram of the MC Ξ^- shape plus a fourth order Legendre polynomial background function. Here and below the χ^2 method is used for fitting.

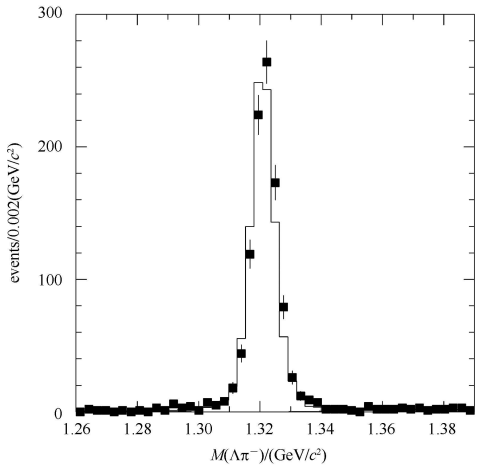

Fig. 3. The fitting result for the $\Lambda\pi^-$ mass distribution. The signal is fitted with the $\Lambda\pi^-$ Monte Carlo shape, and the background with a fourth order Legendre Polynomial.

The $\bar{\Lambda}\pi^+$ Invariant mass is plotted in Fig. 4, requiring $|M(\Lambda\pi^-)-1.321|<0.012$ GeV/c^2 to select the signal and $|M(\bar{\Lambda}\pi^-)-1.383|>0.054$ GeV/c^2 and $|M(\Lambda\pi^+)-1.383|>0.054$ GeV/c^2 to veto $\mathrm{J/\psi}\to\Sigma(1385)^+\bar{\Sigma}(1385)^-$. The distribution is fitted with a histogram of the MC $\bar{\Xi}^+$ shape plus a fourth order Legendre polynomial background function.

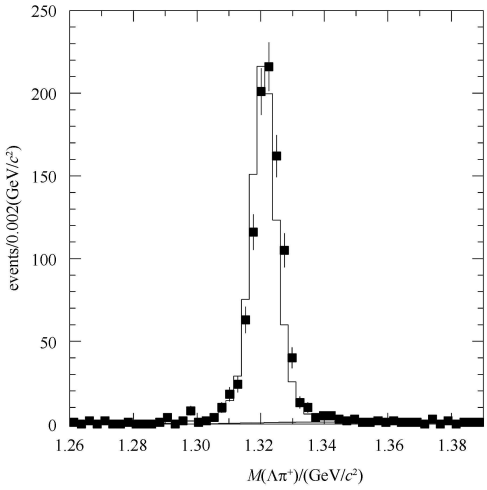

Fig. 4. The fitting result for the $\bar{\Lambda}\pi^+$ mass distribution. The signal is fitted with the $\bar{\Lambda}\pi^+$ Monte Carlo shape, and for the background a fourth order Legendre polynomial is used.

From the fit, the number of signal events for Ξ^- and $\bar{\Xi}^+$ are $N_{\Xi^-}=979\pm35$ and $N_{\bar{\Xi}^+}=942\pm35$, respectively. The number of observed events for $\mathrm{J/\psi}\to\Xi^-\bar{\Xi}^+$ is taken as the average of N_{Ξ^-} and $N_{\bar{\Xi}^+}$, i.e., $N^{\mathrm{obs}}=961\pm35$.

To obtain α for $\mathrm{J/\psi}\to\Xi^-\bar{\Xi}^+$, the angular distribution is corrected with the detection efficiency as $\dfrac{\mathrm{d}N}{\mathrm{d}\cos\theta}\sim f(\cos\theta)(1+\alpha\cos^2\theta)$, where $f(\cos\theta)$ is determined bin by bin from the MC simulation. Background in the distribution is removed using the selection criteria: $|M_{\mathrm{p}\pi^-}-M_\Lambda|<0.008$ GeV/c^2, $|M_{\bar{\mathrm{p}}\pi^+}-M_{\bar{\Lambda}}|<0.008$ GeV/c^2, $|M(\bar{\Lambda}\pi^+)-1.321|<0.009$ GeV/c^2, $|M(\Lambda\pi^-)-1.321|<0.009$ GeV/c^2, $|M(\bar{\Lambda}\pi^-)-1.383|>0.04$ GeV/c^2, $|M(\Lambda\pi^+)-1.383|>0.04$ GeV/c^2. Fitting the efficiency corrected distribution, as shown in Fig. 5, we obtain $\alpha=0.35\pm0.29$ for $\mathrm{J/\psi}\to\Xi^-\bar{\Xi}^+$, where the error is statistical. The fit uses a binned χ^2 minimization method in the angular range $|\cos\theta|\leqslant0.7$.

The detection efficiency for the $\mathrm{J/\psi}\to\Xi^-\bar{\Xi}^+$ is determined to be $\epsilon_{\mathrm{MC}}=(4.50\pm0.04)\%$ by generating MC events with $\alpha=0.35$. The branching fraction is calculated with

$$Br=\frac{N^{\mathrm{obs}}}{N_{\mathrm{J/\psi}}\epsilon_{\mathrm{MC}}Br(\Xi\to\Lambda\pi)^2Br(\Lambda\to\mathrm{p}\pi)^2},\qquad(1)$$

where the branching fractions of $Br(\Xi \to \Lambda\pi) = (99.887\pm0.035)\%$ and $Br(\Lambda \to p\pi) = (63.9\pm0.5)\%$, are taken from the Particle Data Group (PDG) [12], and the number of J/ψ events is $N_{J/\psi} = 57.7 \times 10^6$ [13]. The branching fraction is determined to be:

$$Br(J/\psi \to \Xi^-\bar{\Xi}^+) = (0.90 \pm 0.03) \times 10^{-3},$$

where the error is statistical.

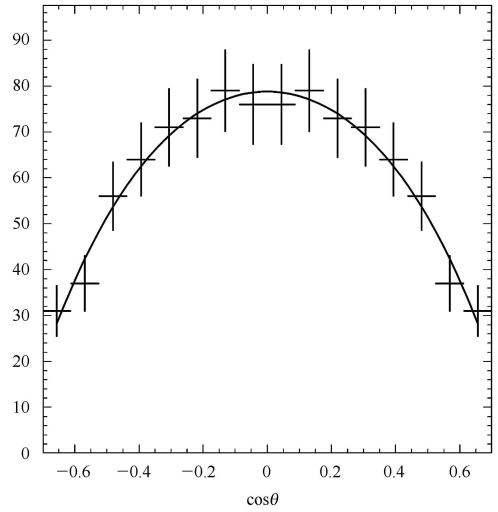

Fig. 5. The angular distribution for the efficiency corrected data of $J/\psi \to \Xi^-\bar{\Xi}^+$. The value of the angular parameter is determined to be $\alpha = 0.35 \pm 0.29$.

4.2 The analysis of $J/\psi \to \Sigma(1385)^-\bar{\Sigma}(1385)^+$

For the decay, $J/\psi \to \Sigma(1385)^-\bar{\Sigma}(1385)^+ \to (\Lambda\pi^-)$ $(\bar{\Lambda}\pi^+) \to (\bar{p}\pi^-\pi^-)$ $(\bar{p}\pi^+\pi^+)$, $\Sigma(1385)^-$ $(\bar{\Sigma}(1385)^+)$ candidates are reconstructed from the selected $\Lambda\pi^-(\bar{\Lambda}\pi^+)$, and the $\Lambda(\bar{\Lambda})$ selection criteria are the same as above.

The $\Lambda\pi^-$ invariant mass is plotted in Fig. 6 requiring $1.333 < M(\bar{\Lambda}\pi^+) < 1.441$ GeV/c^2 to select the signal and $|M(\Lambda\pi^+) - 1.383| > 0.054$ GeV/c^2 and $|M(\bar{\Lambda}\pi^-) - 1.383| > 0.054$ GeV/c^2 to veto $J/\psi \to \Sigma(1385)^+\bar{\Sigma}(1385)^-$. The distribution is fitted with a histogram of the MC $\Sigma(1385)^-$ shape plus a fourth order Legendre polynomial background function.

The $\bar{\Lambda}\pi^+$ invariant mass distribution is plotted in Fig. 7 requiring $1.333 < M(\Lambda\pi^-) < 1.441$ GeV/c^2 to select the signal and $|M(\Lambda\pi^+) - 1.383| > 0.054$ GeV/c^2 and $|M(\bar{\Lambda}\pi^-) - 1.383| > 0.054$ GeV/c^2 to veto $J/\psi \to \Sigma(1385)^+\bar{\Sigma}(1385)^-$. The distribution is fitted with a histogram of the $\bar{\Sigma}(1385)^+$ MC shape plus a background function, a fourth order Legendre polynomial.

The numbers of events obtained from the fits are $N_{\Sigma(1385)^-} = 839 \pm 50$ and $N_{\bar{\Sigma}(1385)^+} = 830 \pm 50$. The observed number of events is taken as the average of $\Sigma(1385)^-$ and $\bar{\Sigma}(1385)^+$, ie., $N^{obs} = 835 \pm 50$.

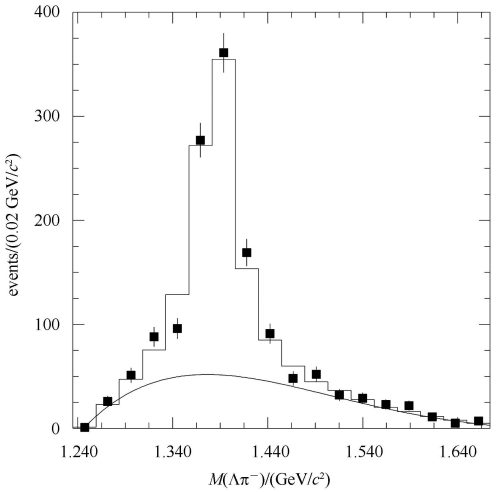

Fig. 6. The fitting result for the $\Lambda\pi^-$ mass distribution. The signal is fitted with the $\Sigma(1385)^-$ Monte Carlo shape and the background is described by a fourth order Legendre polynomial.

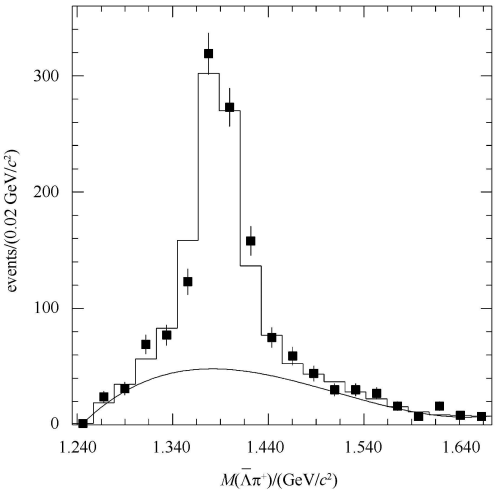

Fig. 7. The fitting results for the $\bar{\Lambda}\pi^+$ mass distribution. The signal is fitted with the $\bar{\Sigma}(1385)^+$ Monte Carlo shape and for the background, a fourth order Legendre polynomial is used.

In order to obtain α for $J/\psi \to \Sigma(1385)^-\bar{\Sigma}(1385)^+$, we use the same procedure as described above. The background can be removed by using the selection criteria: $|M_{p\pi^-} - M_\Lambda| < 0.008$ GeV/c^2, $|M_{\bar{p}\pi^+} - M_{\bar{\Lambda}}| < 0.008$ GeV/c^2, $|M(\bar{\Lambda}\pi^+) - 1.387| < 0.04$ GeV/c^2, $|M(\Lambda\pi^-) - 1.387| < 0.04$ GeV/c^2, $|M(\bar{\Lambda}\pi^-) - 1.383| > 0.04$ GeV/c^2, $|M(\Lambda\pi^+) - 1.383| > 0.04$ GeV/c^2. The MC simulation shows that the efficiency of the BESII detector drops rapidly when $|\cos\theta| > 0.7$, where θ is the angle between $\Sigma(1385)^-$ direction and the positron beam. The same selection

criteria are used for MC and data. Fitting the efficiency corrected distribution is shown in Fig. 8. We obtain $\alpha = -0.54 \pm 0.22$; here the error is statistical only. The fit uses a binned χ^2 minimization method in the angular range $|\cos\theta| \leqslant 0.7$.

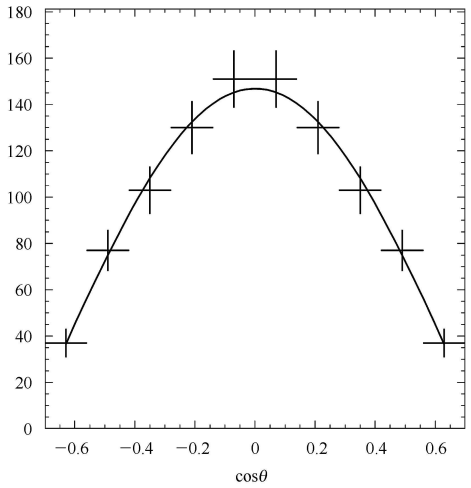

Fig. 8. The angular distribution for the efficiency corrected distribution for $J/\psi \to \Sigma(1385)^-\bar{\Sigma}(1385)^+$. The value of α is -0.54 ± 0.22.

The $J/\psi \to \Sigma(1385)^-\bar{\Sigma}(1385)^+$ efficiency is determined to be $\epsilon_{\rm MC} = (3.80 \pm 0.06)\%$ by generating MC events with $\alpha = -0.54$. Then the branching fraction is calculated by

$$Br = \frac{N^{\rm obs}}{N_{J/\psi}\epsilon_{\rm MC} Br(\Sigma(1385) \to \Lambda\pi)^2 Br(\Lambda \to {\rm p}\pi)^2}, \quad (2)$$

where the branching fractions of $Br(\Sigma(1385) \to \Lambda\pi) = 87.0\%$ and $Br(\Lambda \to {\rm p}\pi) = 63.9\%$ are taken from the PDG [12] and the number of J/ψ events is $N_{J/\psi} = 57.7 \times 10^6$. The branching fraction is determined to be:

$$Br(J/\psi \to \Sigma(1385)^-\bar{\Sigma}(1385)^+) = (1.23 \pm 0.07) \times 10^{-3},$$

where the error is statistical.

4.3 The analysis of $J/\psi \to \Sigma(1385)^+\bar{\Sigma}(1385)^-$

For $J/\psi \to \Sigma(1385)^+\bar{\Sigma}(1385)^- \to (\Lambda\pi^+)(\bar{\Lambda}\pi^-) \to (\bar{\rm p}\pi^-\pi^+)(\bar{\rm p}\pi^+\pi^-)$, the $\Lambda(\bar{\Lambda})$ candidates are reconstructed from $\rm p\pi^-(\bar{p}\pi^+)$, and the $\Sigma(1385)^+\bar{\Sigma}(1385)^-$ candidates are reconstructed in $\Lambda\bar{\Lambda}\pi^+\pi^-$. The $\Lambda(\bar{\Lambda})$ selection criteria are the same as described above.

The $\Lambda\pi^+$ invariant mass distribution is plotted in Fig. 9 requiring $1.333 < M(\bar{\Lambda}\pi^-) < 1.441$ GeV/c^2 to select signal and ($M(\Lambda\pi^-) < 1.309$ or $M(\Lambda\pi^-) > 1.441$) GeV/c^2 and ($M(\bar{\Lambda}\pi^+) < 1.309$ or $M(\bar{\Lambda}\pi^+) > 1.441$) GeV/$c^2$ to veto $J/\psi \to \Xi^-\bar{\Xi}^+$ and $J/\psi \to \Sigma(1385)^-\bar{\Sigma}(1385)^+$. The distribution is fitted with a histogram of the $\Sigma^+(1385)$ MC shape plus a background function, a fourth order Legendre polynomial.

The $\bar{\Lambda}\pi^-$ invariant mass distribution is plotted in Fig. 10 requiring $1.333 < M(\Lambda\pi^+) < 1.441$ GeV/c^2 to select the signal and ($M(\Lambda\pi^-) < 1.309$ or $M(\Lambda\pi^-) > 1.441$) GeV/c^2 and ($M(\bar{\Lambda}\pi^+) < 1.309$ or $M(\bar{\Lambda}\pi^+) > 1.441$) GeV/$c^2$ to veto $J/\psi \to \Xi^-\bar{\Xi}^+$ and $J/\psi \to \Sigma(1385)^-\bar{\Sigma}(1385)^+$. The distribution is fitted with a histogram of the $\bar{\Sigma}(1385)^-$ MC shape plus a fourth order Legendre polynomial to describe the background.

The numbers of events obtained from the fits are $N_{\Sigma(1385)^+} = 1005 \pm 53$ and $N_{\bar{\Sigma}(1385)^-} = 1060 \pm 59$. The final observed number of events is taken as the average of $\Sigma(1385)^+$ and $\bar{\Sigma}(1385)^-$, i.e., $N^{\rm obs} = 1033 \pm 56$.

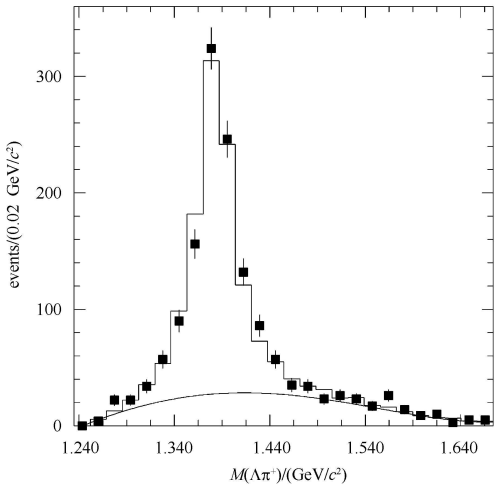

Fig. 9. The fitting result for the $\Lambda\pi^+$ mass distribution. The distribution is fitted with the $\Sigma(1385)^+$ Monte Carlo shape and a fourth order Legendre polynomial to describe the background.

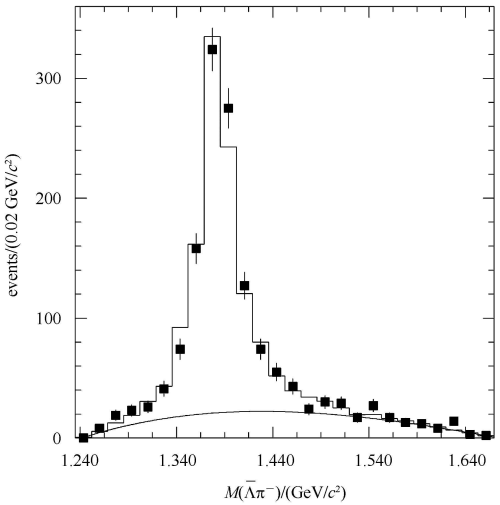

Fig. 10. The fitting result for the $\bar{\Lambda}\pi^-$ mass distribution. The distribution is fitted with the $\bar{\Sigma}(1385)^-$ Monte Carlo shape and a fourth order Legendre polynomial for the background.

To obtain the parameter α for $J/\psi \to \Sigma(1385)^+\bar{\Sigma}(1385)^-$, the same procedure as above is adopted. The fit of the distribution, corrected for the selection efficiency, is shown in Fig. 11. We obtain $\alpha = -0.35 \pm 0.25$, where the error is statistical only. The fit uses a binned χ^2 minimization method in the angular range $|\cos\theta| \leqslant 0.7$.

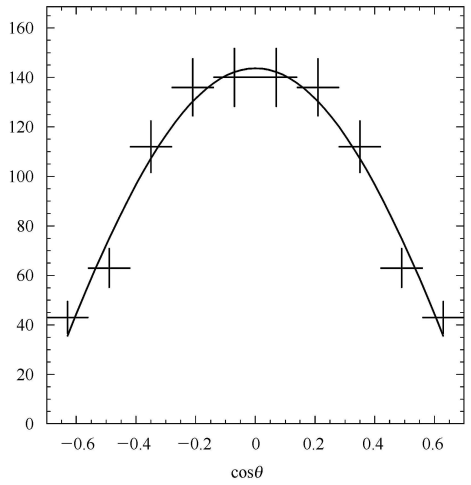

Fig. 11. The angular distribution for the efficiency corrected $J/\psi \to \Sigma(1385)^+\bar{\Sigma}(1385)^-$ events. The value of $\alpha = -0.35 \pm 0.25$ is obtained.

The $J/\psi \to \Sigma(1385)^+\bar{\Sigma}(1385)^-$ efficiency is determined to be $\epsilon_{\rm MC} = (3.83 \pm 0.08)\%$ by generating the MC events with $\alpha = -0.35$. The branching fraction, calculated with Eq. (2), is determined to be:

$$Br(J/\psi \to \Sigma(1385)^+\bar{\Sigma}(1385)^-) = (1.50 \pm 0.08) \times 10^{-3},$$

where the error is statistical only.

5 Branching fraction of $J/\psi \to \Lambda\bar{\Lambda}\pi^+\pi^-$

The Λ invariant mass distribution is plotted in Fig. 12 after requiring $|M_{\bar{\rm p}\pi^+} - M_{\bar{\Lambda}}| < 0.008$ GeV/c^2 and $|M(\bar{\Lambda}\pi^+) - 1.321| > 0.012$ GeV/c^2, $|M(\Lambda\pi^-) - 1.321| > 0.012$ GeV/c^2, $|M(\bar{\Lambda}\pi^+) - 1.387| > 0.054$GeV/$c^2$, $|M(\Lambda\pi^-) - 1.387| > 0.054$ GeV/c^2, $|M(\bar{\Lambda}\pi^-) - 1.383| > 0.054$ GeV/c^2, and $|M(\Lambda\pi^+) - 1.383| > 0.054$ GeV/c^2 to exclude $J/\psi \to \Xi^+\bar{\Xi}^-$, $J/\psi \to \Sigma(1385)^-\bar{\Sigma}(1385)^+$, and $J/\psi \to \Sigma(1385)^+\bar{\Sigma}(1385)^-$. The distribution is fitted by a histogram of the signal shape from MC and a third order Legendre polynomial for the background.

The $\bar{\Lambda}$ invariant mass is plotted in Fig. 13 requiring $|M_{\rm p\pi^-} - M_{\Lambda}| < 0.008$ GeV/c^2 to select the signal and $|M(\bar{\Lambda}\pi^+) - 1.321| > 0.012$ GeV/c^2, $|M(\Lambda\pi^-) - 1.321| > 0.012$ GeV/c^2, $|M(\bar{\Lambda}\pi^+) - 1.387| > 0.054$ GeV/c^2, $|M(\Lambda\pi^-) - 1.387| > 0.054$ GeV/c^2, $|M(\bar{\Lambda}\pi^-) - 1.383| > 0.054$ GeV/c^2, and $|M(\Lambda\pi^+) - 1.383| > 0.054$ GeV/c^2 to exclude $J/\psi \to \Xi^+\bar{\Xi}^-$, $J/\psi \to \Sigma(1385)^-\bar{\Sigma}(1385)^+$, and $J/\psi \to \Sigma(1385)^+\bar{\Sigma}(1385)^-$. The distribution is fitted with a histogram of the Λ MC shape plus a third order Legendre polynomial background function.

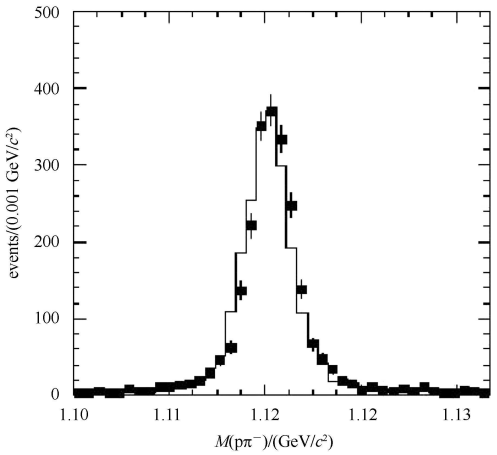

Fig. 12. The fitting results for the $p\pi^-$ mass distribution. The distribution is fitted with the Λ Monte Carlo shape and a third order Legendre polynomial is used to describe the background.

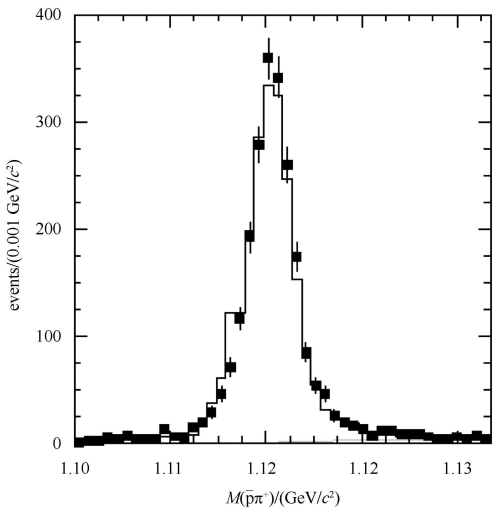

Fig. 13. The fitting results for the $\bar{p}\pi^+$ mass distribution. The signal is fitted with the $\bar{\Lambda}$ Monte Carlo shape and the background with a third order Legendre polynomial.

The number of Λ and $\bar{\Lambda}$ events obtained from the fits are $N_{\Lambda} = 2443 \pm 68$ and $N_{\bar{\Lambda}} = 2287 \pm 72$, respectively. The final observed number of events is taken as the average of the N_{Λ} and $N_{\bar{\Lambda}}$, i.e., $N^{\rm obs} = 2365 \pm 70$, and the MC detection efficiency for $J/\psi \to \Lambda\bar{\Lambda}\pi^+\pi^-$ is $\epsilon_{\rm MC} = (5.27 \pm 0.05)\%$.

Table 1. Measured results for the branching fraction of $J/\psi \to \Lambda\bar{\Lambda}\pi^+\pi^-$, $J/\psi \to \Xi^-\bar{\Xi}^+$, $J/\psi \to \Sigma(1385)^-\bar{\Sigma}(1385)^+$ and $J/\psi \to \Sigma(1385)^+\bar{\Sigma}(1385)^-$.

$J/\psi \to$	our result ($\times 10^{-3}$)	other sources ($\times 10^{-3}$)
$\Lambda\bar{\Lambda}\pi^+\pi^-$	$4.30 \pm 0.13 \pm 0.99$	—
$\Xi^-\bar{\Xi}^+$	$0.90 \pm 0.03 \pm 0.18$	(0.85 ± 0.16) PDG value [12]
$\Sigma(1385)^-\bar{\Sigma}(1385)^+$	$1.23 \pm 0.07 \pm 0.30$	(1.03 ± 0.13) PDG value [12]
$\Sigma(1385)^+\bar{\Sigma}(1385)^-$	$1.50 \pm 0.08 \pm 0.38$	$(1.03 \pm 0.24 \pm 0.25)$ MARK II [1]

Table 2. α values for $J/\psi \to \Xi^-\bar{\Xi}^+$, $J/\psi \to \Sigma(1385)^-\bar{\Sigma}(1385)^+$ and $J/\psi \to \Sigma(1385)^+\bar{\Sigma}(1385)^-$.

$J/\psi \to$	our result	other sources
$\Xi^-\bar{\Xi}^+$	$0.35 \pm 0.29 \pm 0.06$	-0.13 ± 0.59 (MARK II) [1]
$\Sigma(1385)^-\bar{\Sigma}(1385)^+$	$-0.54 \pm 0.22 \pm 0.10$	—
$\Sigma(1385)^+\bar{\Sigma}(1385)^-$	$-0.35 \pm 0.25 \pm 0.06$	—

The branching fraction is calculated using:

$$Br = \frac{N^{\rm obs}}{N_{J/\psi} Br(\Lambda \to p\pi)^2}. \quad (3)$$

The branching fraction excluding $J/\psi \to \Xi^+\bar{\Xi}^-$, $J/\psi \to \Sigma(1385)^-\bar{\Sigma}(1385)^+$, and $J/\psi \to \Sigma(1385)^+\bar{\Sigma}(1385)^-$ is determined to be:

$$Br(J/\psi \to \Lambda\bar{\Lambda}\pi^+\pi^-) = (4.30 \pm 0.13) \times 10^{-3},$$

where 0.13 is the statistical error.

6 The systematic errors of the angular distribution

Using different MDC wire resolution models in the MC simulations, the systematic errors on α in J/ψ decays into $\Xi^-\bar{\Xi}^+$, $\Sigma(1385)^-\bar{\Sigma}(1385)^+$, and $\Sigma(1385)^+\bar{\Sigma}(1385)^-$ from the tracking reconstruction are determined to be 15.2%, 15.8% and 14.9%, respectively. If the efficiency correction curve is changed by 1σ for these three decays, the α values are changed by 7.4%, 8.8% and 8.9%, respectively. The effects of background uncertainties on α are negligible. Adding these contributions for J/ψ decays into $\Xi^-\bar{\Xi}^+$, $\Sigma(1385)^-\bar{\Sigma}(1385)^+$ and $\Sigma(1385)^+\bar{\Sigma}(1385)^-$ in quadrature gives total systematic errors of 16.9%, 18.1% and 17.4%, respectively. The absolute values for the α uncertainty are given in Table 2.

7 The systematic errors for branching fractions

The systematic errors on the branching fractions are dominated by uncertainties of the MDC tracking, particle identification (PID), MC simulation model, background uncertainty, kinematic fit, secondary branching fraction, α, and the uncertainty of the number of J/ψ events.

7.1 The MDC tracking

The MDC tracking efficiency has been measured using channels like $J/\psi \to \rho\pi$, $J/\psi \to \Lambda\bar{\Lambda}$, and $J/\psi \to \mu^+\mu^-$. The MC simulation agrees with data within 1% to 2% for each charged track [11]. In the decay of $J/\psi \to \Lambda\bar{\Lambda}\pi^+\pi^-$, 12% is regarded as the error caused by the tracking efficiency of six charged tracks.

7.2 The particle identification (PID)

The particle identifications of π and p are described in Ref. [11]. In our case, two charged tracks, p and $\bar{p}$, are identified. The systematic error from the particle identification is 4%.

7.3 The background uncertainty

This systematic error arises from the uncertainty of the background shape. Changing the order of the background polynomial and the fitting range gives the systematic error. The errors for $J/\psi \to \Lambda\bar{\Lambda}\pi^+\pi^-$, $J/\psi \to \Xi^-\bar{\Xi}^+$, $J/\psi \to \Sigma(1385)^-\bar{\Sigma}(1385)^+$, and $J/\psi \to \Sigma(1385)^+\bar{\Sigma}(1385)^-$ are 0.12%, 1.10%, 0.54% and 4.70%, respectively.

7.4 The MC model

Different simulation models for the hadronic interaction (GCALOR/FLUKA) give different efficiencies, leading to different branching fractions. For π simulation, GCALOR is better than FLUKA; for p simulation FLUKA is better than GCALOR in the lower momentum region. So, in our analysis, all the baryons and anti-baryons are simulated by the GCALOR model and the difference between GCALOR and FLUKA is taken as the systematic error of the hadronic interaction model. The system-

atic error for the MC efficiencies for $J/\psi \to \Lambda\bar{\Lambda}\pi^+\pi^-$ is 17.5% and the errors for the intermediate resonances, $J/\psi \to \Xi^-\bar{\Xi}^+$, $J/\psi \to \Sigma(1385)^-\bar{\Sigma}(1385)^+$, and $J/\psi \to \Sigma(1385)^+\bar{\Sigma}(1385)^-$ are 12.9%, 18.4% and 19.8%, respectively.

7.5 Variations of selection requirements

The sensitivity to our selection requirement values has been determined by varying all selection requirements used by +6%. The corresponding differences for each variation have been combined in quadrature to obtain the total uncertainty corresponding to our requirement values. The systematic errors for variations in the requirements for $J/\psi \to \Lambda\bar{\Lambda}\pi^+\pi^-$, $J/\psi \to \Xi^-\bar{\Xi}^+$, $J/\psi \to \Sigma(1385)^-\bar{\Sigma}(1385)^+$ and $J/\psi \to \Sigma(1385)^+\bar{\Sigma}(1385)^-$ are 1.30%, 0.45%, 0.21% and 0.46%, respectively.

7.6 Intermediate decay branching fractions

The errors on the branching fractions of $\Xi \to \Lambda\pi$, $\Sigma(1385) \to \Lambda\pi$ and $\Lambda \to p\pi$ decays are 0.035%, 1.5% and 0.5%, respectively. These values are taken from the Particle Data Group [12].

7.7 Effect of α on the detection efficiency

When we change α by 1σ, the detection efficiencies for $J/\psi \to \Xi^-\bar{\Xi}^+$, $J/\psi \to \Sigma(1385)^-\bar{\Sigma}(1385)^+$ and $J/\psi \to \Sigma(1385)^+\bar{\Sigma}(1385)^-$ are changed by 1.2%, 5.7% and 0, respectively. These are taken as the systematic errors due to α.

7.8 The kinematic fit

The 4C-kinematic fit error is studied using $J/\psi \to \Xi^-\bar{\Xi}^+$. The Monte Carlo events are generated using phase space, the analysis is performed with and without the 4C-fit both in data and MC, and the relative efficiency difference between these two cases is 6%.

7.9 The number of J/ψ events

The number of J/ψ events is $(57.7\pm2.72)\times10^6$ [13], so we take 4.7% as the systematic error on the number of J/ψ events.

Combining the uncertainties from all sources in quadrature, the total systematic errors of the branching fractions of $J/\psi \to \Lambda\bar{\Lambda}\pi^+\pi^-$, $J/\psi \to \Xi^-\bar{\Xi}^+$, $J/\psi \to \Sigma(1385)^-\bar{\Sigma}(1385)^+$, and $J/\psi \to \Sigma(1385)^+\bar{\Sigma}(1385)^-$ are 23.41%, 20.24%, 24.97%, and 25.82%, respectively.

8 Summary

Using 5.77×10^7 J/ψ events taken by the BES II detector at the BEPC, we have measured the branching fraction of $J/\psi \to \Lambda\bar{\Lambda}\pi^+\pi^-$ for the first time, and the branching fractions for $J/\psi \to \Xi^-\Xi^+, \Sigma(1385)^-\bar{\Sigma}(1385)^+$, and $\Sigma(1385)^+\bar{\Sigma}(1385)^-$ are measured with improved precision. The branching fraction for $J/\psi \to \Lambda\bar{\Lambda}\pi^+\pi^-$ is $(4.30\pm0.13\pm0.99)\times10^{-3}$. The comparison between our result and the PDG values is given in Table 1.

The angular distribution for $J/\psi \to B\bar{B}$ has been studied. As shown in Table 2, the parameters of α, describing the baryon angular distribution in the form $\frac{dN}{d\cos\theta} \sim (1+\alpha\cos^2\theta)$ for the modes of $J/\psi \to \Xi^-\bar{\Xi}^+$, $\Sigma(1385)^-\bar{\Sigma}(1385)^+$, and $\Sigma(1385)^+\bar{\Sigma}(1385)^-$ are measured for the first time.

The BES collaboration would like to thank the staff at BEPC and Computing Center for their hard work.

References

1 Eaton M W et al. Phys. Rev. D, 1984, **29**: 804
2 Henrard P et al. Nucl. Phys. B, 1987, **292**: 670–692
3 Abilkim M et al. (BES collaboration). Phys. Lett. B, 2006, **632**: 181–186
4 Herber H E, Perrier J. Phys. Rev. D, 1985, **32**: 2961
5 BAI J Z et al. (BES collaboration). Phys. Lett. B, 2004, **591**: 42
6 Ablikim M et al. (BES collaboration). Phys. Lett. B, 2007, **648**: 149
7 CHEN Hong, PING R G. Phys. Lett. B, 2007, **644**: 54–58
8 Carimalo C. Int. J. Mod. Phys. A, 1987, **2**: 249
9 BAI J Z et al. (BES collaboration). Nucl. Instrum. Methods A, 1994, **344**: 319
10 BAI J Z et al. (BES collaboration). Nucl. Instrum. Methods A, 2001, **458**: 627
11 Ablikim M et al. (BES collaboration). Nucl. Instrum. Methods A, 2005, **552**: 344
12 YAO W M et al. (Particle Data Group). Journal of Physics G, 2012, **33**: 1 (on the web)
13 FANG S S et al. High Energy Phys. and Nucl. Phys., 2003, **27**: 277 (in Chinese)